Opponent thermosensory cells use flexible cross-inhibition for context-dependent choice in *Drosophila* thermotaxis

Luis Hernandez-Nunez[1,2,3], Alicia Chen[1,2,4], Gonzalo Budelli[5,6,7], Vincent Richter[9], Anna Rist[9], Andreas S. Thum[9], Mason Klein[8], Paul Garrity[5,6,7], and Aravinthan D.T. Samuel[1,2]

[1]Department of Physics, Harvard University, Cambridge, MA 02138, USA, [2]Center for Brain Science, Harvard University, Cambridge, MA 02138, USA, [3]Systems, Synthetic, and Quantitative Biology PhD program, Harvard University, Cambridge, United States, [4]Harvard College, Harvard University, Cambridge, MA 02138, USA, [5]National Center for Behavioral Genomics, Brandeis University, Waltham, United States, [6]Department of Biology, Brandeis University, Waltham, United States, [7]Volen Center for Complex Systems, Brandeis University, Waltham, United States, [8]Department of Physics, University of Miami, Coral Gables,FL, United States, [9]University of Leipzig, Institute of Biology, Talstraße 33, 04103 Leipzig, Germany

Animals often use sensory cells with opposing polarity that are separately tuned to detect increments or decrements of environmental stimuli. For example, cooling and warming cells detect temperature changes;[1,2] moist and dry cells detect humidity changes;[3,4] and ON-OFF retinal cells detect luminance changes.[5,6] How animals integrate the outputs of opponent cells to navigate towards favorable points along a sensory gradient from higher or lower points remains poorly understood. Here, we show how the outputs of warming cells (WCs) and cooling cells (CCs) in the *Drosophila* larva are combined to produce context-dependent thermotactic navigation. The newly discovered WCs and the previously described CCs[7] require distinct but overlapping sets of Ionotropic Receptors to sense temperature changes: Ir68a, Ir93a, and Ir25a for WCs; Ir21a, Ir93a, and Ir25a for CCs. WCs and CCs are bidirectional opponent sensors: WCs are activated by warming and inhibited by cooling, whereas CCs are activated by cooling and inhibited by warming. Both WCs and CCs are sensitive to temperature changes from high temperatures where the larva avoids warming to low temperatures where it avoids cooling. However, at all temperatures, optogenetically-imposed fictive warming of the WCs as well as fictive cooling of the CCs evoke avoidance responses, and fictive cooling of the WCs as well as fictive warming of the CCs inhibit avoidance responses. We reconcile these sensory properties and behavioral responses by showing that the larva uses flexible cross-inhibition of the output pathways of WCs and CCs when making perceptual choices during thermotaxis. Balanced cross-inhibition near preferred temperatures suppresses any directed movement on temperature gradients. Above preferred temperatures, WCs mediate avoidance to warming while cross-inhibiting avoidance to cooling. Below preferred temperatures, CCs mediate avoidance to cooling while cross-inhibiting avoidance to warming. Our results show how flexible cross-inhibition orchestrates a context-dependent perceptual choice during a navigational behavior.

Many animals from insects to mammals use specialized thermosensory cells to sense warming or cooling.[8,9] Behavioral responses to warming and cooling are ambient temperature context-dependent: below preferred temperatures cooling should evoke avoidance behaviors, above preferred temperatures warming should evoke avoidance behaviors, and near preferred temperatures any avoidance behavior should be inhibited. Thus, the outputs of thermosensory cells must be used flexibly by behavioral algorithms to orient the animal towards preferred temperatures from higher or lower points on a gradient.

Previous studies, in *Caenorhabditis elegans*,[10] larval and adult *Drosophila melanogaster*,[9] larval zebrafish[11,12] and rodents[8] have focused on the physiology of single thermosensory cell types and their contribution to behavioral responses in a specific temperature context. Deriving a behavioral algorithm that incorporates the flexibility needed to make decisions in different temperature contexts requires determining how an animal integrates the contributions of all relevant thermosensory cell types to navigation at all temperatures.

Here, we investigate the sensory cells and behavioral algorithms that guide *Drosophila* larva thermotaxis towards preferred temperatures (near 24°C), and away from high or low temperatures. Previous work uncovered three anterior cooling cells (CCs) in the Dorsal Organ Ganglion (DOG) that are required for cold avoidance from as low as 14°C towards 24°C.[7] The CCs are not required for warm avoidance above 24°C. The CCs are activated by cooling and inhibited by warming in a surprisingly large range from 14°C to 34°C. Two A-type CCs have uniform sensitivity to temperature changes from 14 to 34°C, and one B-type CC has slightly less sensitivity above 25°C.[7] Thus, the CCs are activated by cooling near 24°C where the larva has a neutral behavioral response to temperature changes, and are also activated by cooling above 24°C where it exhibits warm avoidance.

Understanding thermotaxis in the *Drosophila* larva requires identifying additional thermosensory cells and understanding how the outputs of different thermosensory cells are combined to make behavioral decisions at all temperatures. Here, we uncover warming cells (WCs) with close morphological and genetic similarity to the previously described CCs. Using optogenetics, calcium imaging, precise temperature control, sensory receptor mutants, and quantitative behavioral analysis, we derive a behavioral algorithm for thermotaxis that uses ambient temperature context-dependent cross-inhibition between the simultaneous outputs of the opponent sensory cells. Flexible cross-inhibition allows the net effect of WC and CC output pathways to drive cold avoidance below 24°C, suppress avoidance to temperature changes near 24°C, and drive warm avoidance above 24°C. Our study shows how context-dependent decision-making towards a preferred temperature is encoded in a predictive model of thermotactic behavior that integrates the simultaneous outputs of opponent sensory cells to regulate avoidance responses.

Identifying warming cells

To identify the warming-responsive counterparts of the cooling cells (CCs), we used *in vivo* calcium imaging, expressing GCaMP6m[13] under the control of the pebbled-Gal4 driver that labels all anterior sensory cells in the larva.[14] We subjected larvae to sinusoidal temperature waveforms, volumetrically imaged all anterior sensory ganglia, and used constrained non-

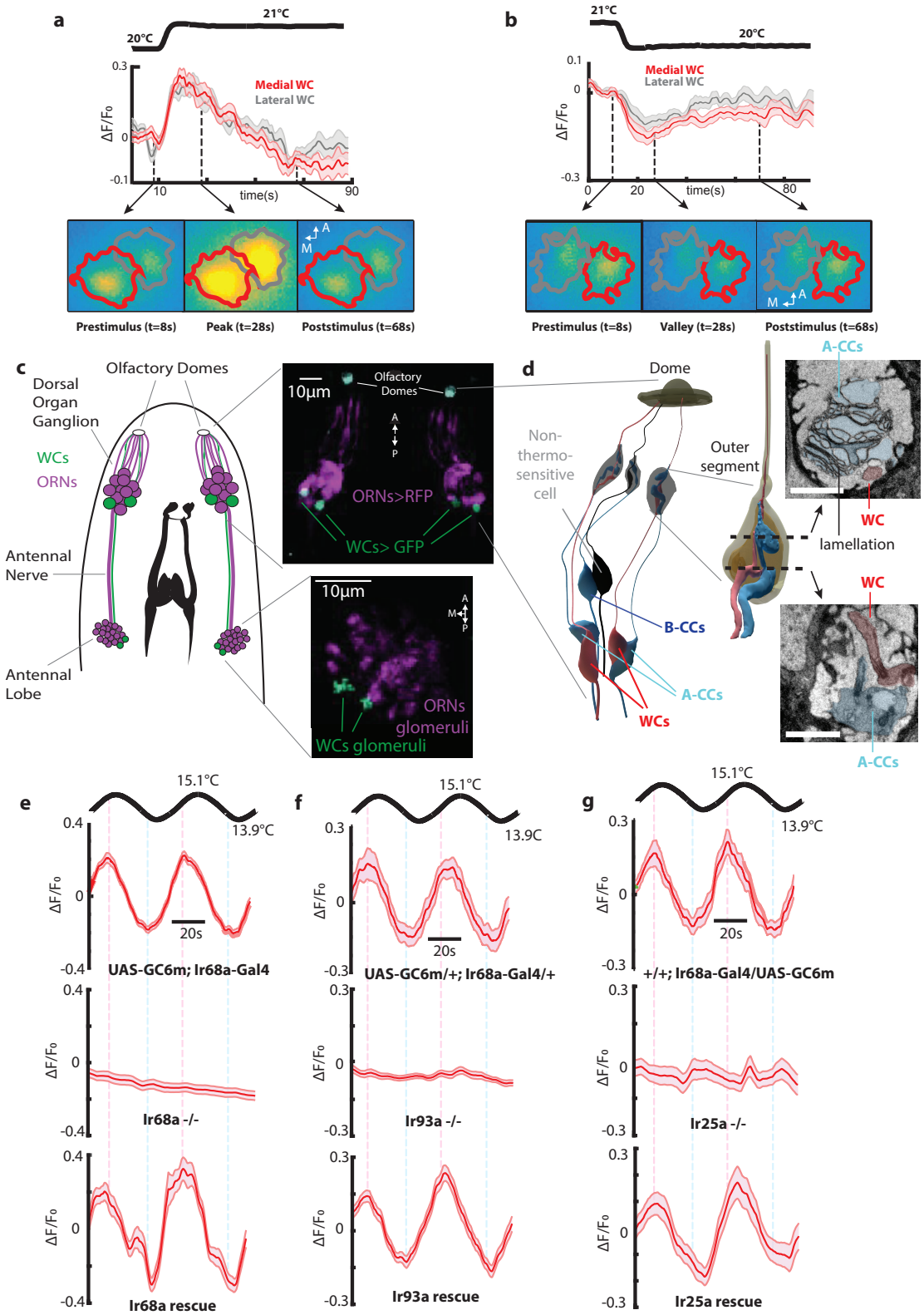

Figure 1. | **The cellular and molecular basis of peripheric warming sensing.** **a-b**, Warming Cells (WCs) are phasic bipolar sensors. **a**, **b**, *Drosophila* larvae expressing GCaMP6m in the WCs (UAS-GCaMP6m;Ir68a-Gal4) calcium response to a 1°C temperature increase (**a**) or decrease (**a**). (n=12 larvae, the shaded regions are the s.e.m.). The medial WC is in red and the lateral WC in grey in the calcium response curves and in the bottom insets that show the CNMF borders for the medial and lateral WC before, during, and after temperature stimulation. **c**,**d**, Anatomy of the WCs. **c**,Larvae expressing GFP in the WCs and RFP in the ORNs (UAS-GFP;Ir68a-Gal4/orco-RFP) imaged in the DOG (cell bodies) and the antennal lobe (axon terminals). **d**, Electron microscopy reconstruction of the thermosensory dendritic bulbs shared by CCs and WCs (scale bars= 1μ m). The top inset shows a section in the lamellated outer segment and the bottom inset shows an unlamellated part of WCs and CCs dendritic processes before the outer segment. **e-g**, Ir68a, Ir93a, and Ir25a are required for warming sensing. Fluorescence changes in the WCs of larvae with different genotypes exposed to a sine wave of temperature. **f**, Wildtype: UAS-GCaMP6m;Ir68a-Gal4 (n=8 animals), Ir68a defective mutants: UAS-GCaMP6m; Ir68a^{PB},Ir68a-Gal4 (n=8 animals), Ir68a rescue: UAS-GCaMP6m;(Ir68a^{PB},Ir68a-Gal4)/(Ir68a^{PB},UAS-Ir68a) (n=10 animals). **g**, Wildtype: UAS-GCaMP6m/+;Ir68a-Gal4/+ (n=8 animals), Ir93a defective mutants: UAS-GCaMP6m;Ir93a^{MI05555} , Ir68a-Gal4/Ir93a^{MI05555} (n=14 animals), Ir93a rescue: UAS-CaMP6m/+;(Ir93a^{MI05555}, Ir68a-Gal4)/(Ir93a^{MI05555}, UAS-Ir93a) (n=8 animals). **h**, Wildtype: +;Ir68a-Gal4/UAS-GCaMP6m (n=8 animals), Ir25a defective mutants: Ir25a^{2};Ir68a-Gal4/UAS-GCaMP6m (n=20 animals), Ir25a rescue: (Ir25aBAC, Ir25a^{2})/Ir25a^{2};Ir68a-Gal4/UAS-GCaMP6m (n=20 animals). Shaded regions are the s.e.m.

negative matrix factorization (CNMF)[15] to analyze activity patterns for evidence of temperature-sensitive cells. CNMF uncovered two novel warming cells (WCs) in the DOG, and also identified the three CCs. No other temperature-sensitive cells were apparent in any anterior sensory ganglia (Supplementary Fig. 1).

We sought cell-specific labels for the WCs. CCs in both adult and larval *Drosophila* express Ionotropic Receptors.[16–18] We screened Ir genes known to be expressed in the DOG, and found that Ir68a-Gal4 exclusively labels the WCs (Supplementary Fig. 2, 3 and Extended Methods). With cell-specific labeling of the WCs using GCaMP6m, we quantified the sensitivity and dynamics of their temperature-evoked responses. A warming step evoked a transient increase in calcium levels that adapted to baseline (Fig. 1a). A cooling step evoked a transient decrease before adaptation to baseline (Fig. 1b). The temperature-evoked calcium dynamics of the two WCs were indistinguishable. Thus, the WCs are bidirectional phasic sensors of temperature change, activated by warming and inhibited by cooling. The CCs are also bidirectional phasic sensors, but activated by cooling and inhibited by warming.[7] Thus, the WCs and CCs represent opponent sensory cells.

Thermosensory cells in many animals have specialized morphologies that presumably enhance temperature detection.[19–21] We used confocal and electron microscopy to reconstruct the anatomy of the WCs and CCs to better understand any structural similarities. Both WCs and CCs are located in the DOG, which mostly contains olfactory receptor neurons that project to different glomeruli in the antennal lobe.[22] We found that each WC projects to a distinct warming glomerulus (Fig. 1c). The CCs project to a single cooling glomerulus.[7] Thermosensory glomeruli lay posterior and dorsal to the olfactory glomeruli.

Knowing the locations of the WCs and CCs, we were able to reconstruct them using electron microscopy (Extended Methods). We found that the cell bodies and outer segments of the A-type CCs and WCs are adjacent (Fig. 1d). The outer segments of the CCs and WCs have specialized morphologies, presumably containing signal transduction machinery. The CC outer segments are large and lamellated with heavily infolded plasma membranes. The WC outer segments are smaller and unlamellated (Fig. 1d inset). These anatomical features are consistent with those of the WCs and CCs of adult *Drosophila*.[21,22] The larval WCs, but not the CCs, also have a thin dendrite that protrudes to the surface of the olfactory dome (Fig. 1d, Supplementary Fig. 4, and Supplementary Material). The cell body and outer segment of the B-type CC are adjacent to a non-thermosensitive cell of the DOG (Supplementary Fig. 1 and Supplementary Material).

The molecular basis of warming sensing

Because Ir68a-Gal4 labels the WCs, we asked whether Ir68a might directly contribute to their thermosensitivity. We confirmed the cell-specific expression of Ir68a in the WCs by examining a Gal4 reporter expressed under the control of the endogenous Ir68a promoter (Ir68a$^{\text{T2A-Gal4}}$).[23] We found that an Ir68a mutation (*Ir68a*^{PB}) abolished temperature-evoked calcium dynamics in the WCs (Fig. 1e). We were able to restore the thermosensitivity of the WCs in the *Ir68a*^{PB} mutant by rescuing cell-specific expression of the wild-type receptor (Fig. 1e).

Most Ionotropic Receptors in *Drosophila* are thought to function as heteromers.[24,25] For example, the CCs require a set of three Ionotropic Receptors to respond to temperature changes: Ir21a, Ir93a, and Ir25a.[16,17] We used Ir21a$^{\text{T2A-Gal4}}$ lines,[23] a reporter of the endogenous Ir21a promoter to drive GFP expression and found that Ir21a expression is specific to the CCs in the entire larva. To map the expression pattern of the Ir93a receptor, we used immunostaining. We found that Ir93a is expressed only in the WCs and CCs (Supplementary Fig. 2). Ir25a is expressed in many anterior sensory cells including the WCs and CCs.[3,16,26,27] We found that mutations in either of the two receptors shared by WCs and CCs, Ir93a (*Ir93a*^{MI}) or Ir25a (*Ir25a*^{2}), abolished WC thermosensitivity (Fig. 1f, g). The thermosensitivity of the WCs in these mutants was restored by rescuing cell-specific expression of the wild-type receptors (Fig. 1f, g).

Our results suggest a model in which distinct but overlapping sets of Ionotropic Receptors confer thermosensitivity to the WCs and CCs. Ir68a is specifically needed by the WCs to sense warming. Ir21a is specifically needed by the CCs to sense cooling. Ir93a is needed by both WCs and CCs to sense any temperature change in the larva. In adult *Drosophila*, Ir93a has been shown to be needed for hygrosensation.[3] Ir25a is more broadly expressed, acting as a co-receptor in many sensory neurons, including gustatory and olfactory neurons, as well as thermo- and hygro-receptors.[24,25] We further tested this model by ectopic expression of Ir68a and Ir21a in the CCs and WCs, respectively. Ectopic expression of Ir68a in the CCs diminished their sensitivity to cooling. Ectopic expression of Ir21a in the WCs transformed them into cooling sensors (Supplementary Fig. 5).

Neural and behavioral responses regulated by opponent thermosensors

Drosophila larvae prefer temperatures near 24°C. Below 24°C, cooling evokes avoidance. Above 24°C, warming evokes avoidance. We sought to map the interplay between ambient temperature, temperature change, thermosensory neuron activity and behavioral response valence. To do this, we developed a temperature control technique to deliver the same temperature waveforms at multiple ambient temperatures during calcium imaging and behavioral experiments (Supplementary Fig. 6 and Extended Methods). We used this setup to quantify the temperature-evoked responses of freely behaving larvae, using an unsupervised classifier to segment behavioral sequences (Supplementary Fig. 7, and Extended Methods). At temperatures where the larva exhibits cold avoidance (<24°C), the most frequent behavioral sequence is turning during cooling. At temperatures for warm avoidance (>24°C), the most frequent behavioral sequence is turning during warming (Supplementary Fig. 7). In all temperature ranges, turning is the avoidance response that helps larvae find a more favorable orientation. Consistent with previous studies of larval navigation,[7,28,29] turning rate captures the valence and intensity of the response to a stimulus.

At preferred temperatures neither warming nor cooling should evoke avoidance behaviors. We subjected larvae to fast as well as slow sinusoidal temperature variations near 24°C. The CCs are activated during the cooling phase and inhibited during the warming phase, whereas the WCs are activated during the warming phase and inhibited during the cooling phase (Fig. 2c). Although neither temperature change should evoke

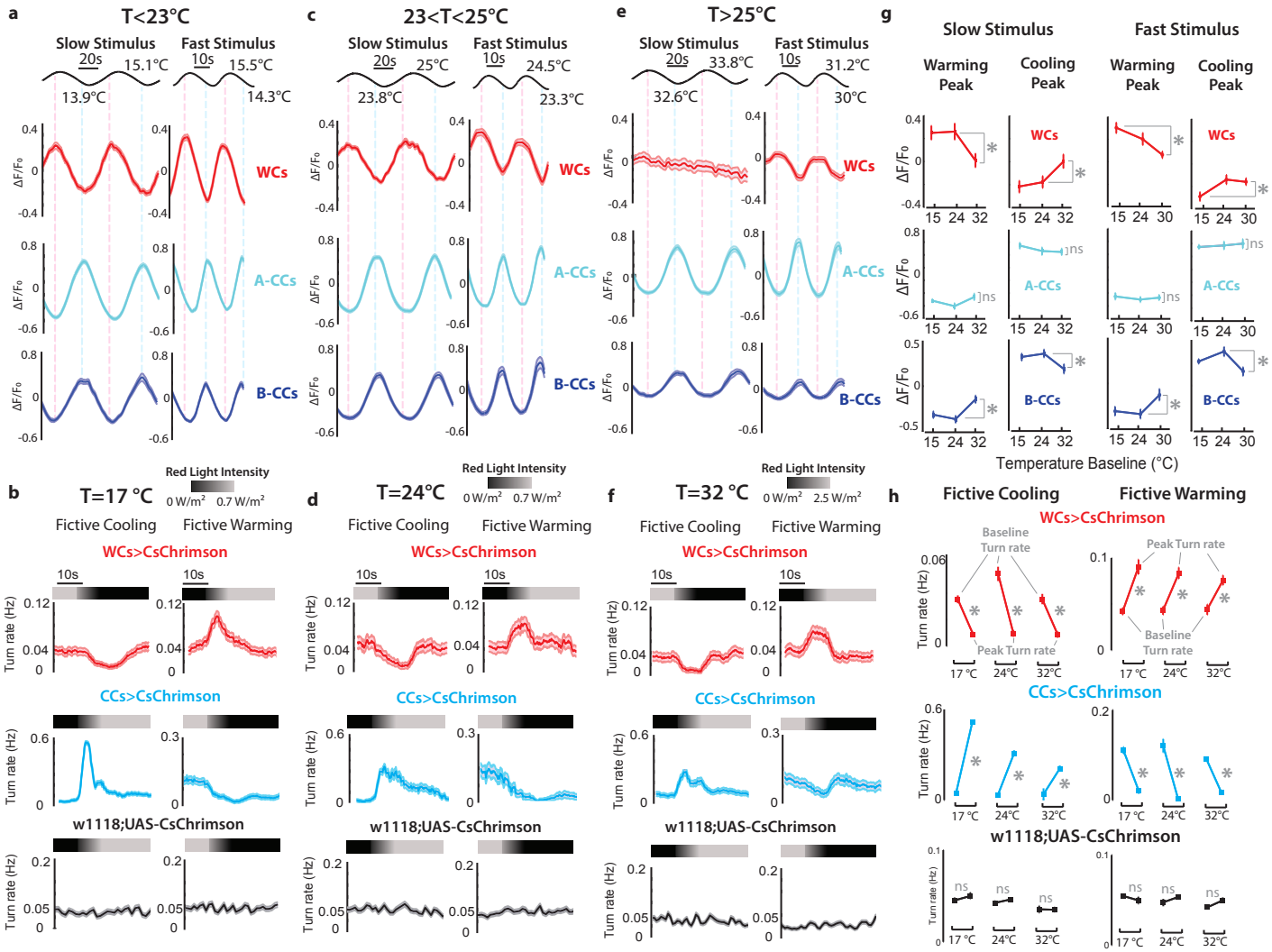

Figure 2. | **Warming and Cooling Cells drive motor programs of opposed valence.** **a**, **c**, **e**, (Top panel) Fluorescence changes in the WCs of Ir68a-Gal4; UAS-GCaMP6m larvae exposed to slow and fast sine waves of temperature centered at low, intermediate, and high temperatures. (red curves, n=8-10 animals, shaded regions are the s.e.m.). (Mid panel) Fluorescence changes in the A-type CCs of R11F02-Gal4; UAS-GCaMP6m larvae exposed to slow and fast sine waves of temperature centered at low, intermediate, and high temperatures. (cyan curves, n=7-10 animals, shaded regions are the s.e.m.). (Bottom panel) Fluorescence changes in the B-type CCs of R11F02-Gal4; UAS-GCaMP6m larvae exposed to slow and fast sine waves of temperature centered at low, intermediate, and high temperatures. (blue curves, n=7-10 animals, shaded regions are the s.e.m.). **b**,**d**, **f**, (Top panel) Turning rate of larvae expressing the red shifted optogenetic channel CsChrimson in the WCs (w^{1118};UAS-CsChrimson/+;Ir68a-Gal4/+) exposed to negative ('fictive cooling') and positive ('fictive warming') ramps of red light. (red curves, n=116-125 animals, shaded regions are the s.e.m.). (Mid panel) Turning rate of larvae expressing the red shifted optogenetic channel CsChrimson in the CCs (w^{1118};UAS-CsChrimson/+;R11F02-Gal4/+) exposed to positive ('fictive cooling') and negative ('fictive warming') ramps of red light. (n=90-101 animals, shaded regions are the s.e.m.). (Bottom panel) Turning rate of control larvae (w^{1118}; UAS-CsChrimson/+) fed with all-trans-retinal (ATR) and exposed to positive and negative ramps of red light. (n=85-120 animals, shaded regions are the s.e.m.). Experiments in **b** were conducted at 17°C, in **d** at 24°C and in **f** at 32°C. **g**, Summary of the positive or negative peak neural responses to cooling and warming. (Top panel) The WCs' positive peak response to warming and negative peak response to cooling are larger at lower and intermediate temperatures and closer to zero at high temperatures. (Mid panel) The A-type CCs positive peak response to cooling and negative peak response to warming are statistically indistinguishable at all temperature baselines. (Bottom panel) The B-type CCs' positive peak response to cooling and negative peak response to warming are closer to zero at high temperatures. The error bars are s.e.m. of the individual neuron responses averaged to calculate the responses displayed in **a**,**c**, **e**. The * indicate that the peak responses between the brackets are different with Kruskal-Wallis test p<0.01. The grey 'ns' indicates no statistically significant difference. **h**, Summary of optogenetic behavioral responses at all temperatures. (Top panel) The peak turning rate in response to optogenetically-imposed cooling (fictive cooling) in the WCs is lower than the baseline at all temperatures, consistent with the WCs inhibiting cooling avoidance. The peak turning rate in response to optogeneticaly-imposed warming is higher than the baseline at all temperatures, consistent with the WCs driving warming avoidance. (Mid panel) The peak turning rate in response to fictive cooling (fictive cooling) in the CCs is higher than the baseline at all temperatures, consistent with the CCs driving cooling avoidance. The peak turning rate in response to fictive warming in the CCs is lower than the baseline at all temperatures, consistent with the CCs inhibiting warming avoidance. (Bottom panel) Control animals fed with ATR display no turning rate increases or decreases at all temperatures. The grey * indicates that the is a statistically significant difference between the peak turn rate and the baseline turn rate (Chi-square test with p<0.001). The grey 'ns' indicates no statistically significant difference.

avoidance near 24°C, WCs and CCs still display strong, opponent physiological responses to temperature change in this range.

Thermosensory stimuli simultaneously affect both WC and CC activity, confounding attempts to distinguish the behavioral consequences of WC versus CC activation. To manipulate WC and CC activity independently, we turned to optogenetics. With cell-specific expression of CsChrimson[30] in either WCs or CCs using controlled optogenetic illumination, we induced fictive temperature changes onto each cell type. Near the larva's preferred temperature, 24°C, we found that increasing optogenetic stimulation of WCs (fictive warming) caused an increase in turning rate (Fig. 2d). In contrast, decreasing optogenetic stimulation of WCs (fictive cooling), caused an decrease in turning rate (Fig. 2d). We observed an opposite pattern with the CCs. Decreasing optogenetic stimulation of the CCs (fictive warming) caused a decrease in turning rate (Fig. 2d). Increasing optogenetic stimulation of CCs (fictive cooling) caused an

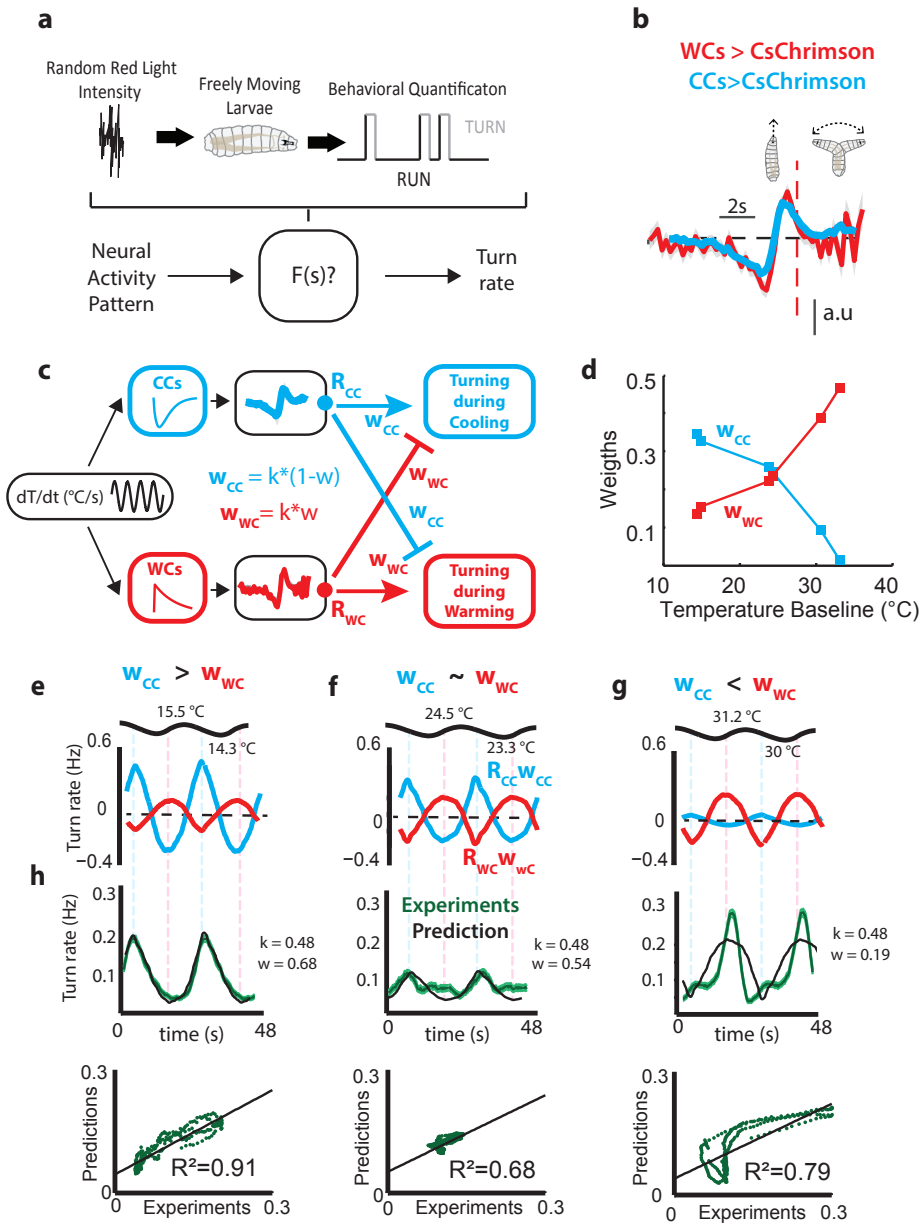

Figure 3. A predictive model of thermotaxis driven by cooling and warming pathways. a, Mapping sensory neurons' activity patterns to behavior. The mathematical function that converts an optogenetic stimulus pattern in a specific type of sensory cells and behavior can be estimated using reverse-correlation of behavioral responses to white noise optogenetic stimulation. In our case this is the transformation from optogenetic activation to turning rate. **b**, Linear filters obtained with white noise optogenetic stimulation of WCs (curve in red) and CCs (curve in cyan). **c**, Schematic representation of the algorithm for thermotactic decision-making. The WCs and CCs outputs are convolved with behavior filters (Extended Methods) and the filter outputs (R_{CC} and R_{WC}) are then combined linearly with the scalar weights w_{CC} and w_{WC}. **d**, At low temperatures, w_{CC} is larger than w_{WC} and consequently the contribution of the CCs is larger than the contribution of the WCs. Near preferred temperatures, in w_{CC} and w_{WC} are close in value and consequently the contribution of the WCs is similar to the contribution of the CCs. At high temperatures, w_{WC} is larger than w_{CC} and consequently the contribution of the WCs is larger than the contribution of the CCs. **e**, **f**, **g**, The outputs of the behavioral filter of the warming pathway (R_{WC}) and the cooling pathway (R_{CC}), scaled by their respective weights (w_{WC} and w_{CC}). This shows how the contribution of the WCs during cooling and the contribution of the CCs during warming is always negative. This is the resulting cross-inhibition of the model. Below preferred temperatures (**e**), to drive cooling avoidance, w_{WC} has to be smaller than w_{CC}. Near preferred temperatures **f**, to suppress avoidance behaviors, w_{WC} and w_{CC} values have to be similar. **g** Above preferred temperatures (**g**), to drive warming avoidance, w_{WC} has to be larger than w_{CC}. **h** (Top panel), Experimental results of the turning rate response to sine waves of temperature of wildtype larvae (w^{1118} in green) and model predictions (in black). Shaded regions around the green curve are then s.e.m. (Bottom panel) Correlations between the model predictions and experimental results at all temperatures.

increase in turning rate (Fig. 2d). Control animals exhibited no behavioral responses to changes in optogenetic stimulation (Fig. 2d).

Thus, although warming and cooling do not evoke avoidance behaviors at preferred temperatures, both WCs and CCs remain physiologically responsive to temperature changes. Moreover, both WCs and CCs continue to regulate behavior, as their optogenetic stimulation evokes motor responses. Near preferred temperatures, an underlying behavioral algorithm must integrate the outputs of the WCs and CCs in a way that inhibits avoidance responses to warming and cooling.

As the behavioral algorithm for thermotaxis must be flexible to both drive warm avoidance above 24°C and cold avoidance below 24°C, we tested physiological and behavioral responses at ambient temperatures above and below 24°C. During cold avoidance, warming has positive behavioral valence and cooling has negative behavioral valence. During warm avoidance, warming has negative behavioral valence and cooling has positive behavioral valence. Using calcium imaging, we found that the CCs are activated by cooling and inhibited by warming with

similar sensitivities at all temperatures (Fig. 2a, c, e, g). Thus, the CCs do not appear to become more sensitive at cold temperatures to upregulate cold avoidance. Similarly, we found that the WCs are activated by warming and inhibited by cooling at all temperatures (Fig. 2a, c, e, g), and are even more sensitive at cold temperatures (Fig. 2a, c, g). Likewise, the WCs do not appear to become more sensitive at warm temperatures to upregulate warm avoidance. The flexibility in the algorithm for thermotaxis is therefore not encoded in the physiological thermosensitivity of WCs and CCs.

We used optogenetics to characterize the behavioral valence associated with the individual activities of the WCs or CCs at cold (17°C) and warm (32°C) temperatures. At all temperatures, fictive cooling applied to the CCs or fictive warming applied to the WCs evokes responses with negative behavioral valence (Fig. 2b, d, f, h). At all temperatures, fictive warming applied to CCs or fictive cooling applied to WCs evokes responses with positive behavioral valence (Fig. 2b, d, f, h). To be able to display warm avoidance, cold avoidance, or inhibit avoidance at preferred temperatures, the larva must flexibly integrate the outputs of the WCs and CCs when determining the behavioral response to warming and cooling.

Flexible cross-inhibition underlies thermotaxis

How does an algorithm integrate the outputs of the WCs and CCs? To uncover the behavioral algorithm from stimulus to motor response, we needed to measure the transformation from WC and CC activity into changes in turning rate. If one provides a linear system with a white-noise sensory stimulus, one can use reverse-correlation analysis to infer the filters that transform neural activity into behavior.[29] We used optogenetic white noise stimulation of the WCs and CCs and reverse-correlation analysis of behavioral responses to infer the filters that transform neural activity into turning rate (Fig. 3a, and Extended Methods). We found that these filters were identical for both WCs and CCs (Fig. 3b). Identical filters suggest that functionally similar pathways transform the activities of the thermosensory cells into behavior.

A linear model for the thermotaxis algorithm is fully determined by knowing how sensory inputs map to WC and CC activity, how WC and CC activities separately map to turning rate, and how sensory inputs map to turning rate. Our datasets span these measurements, allowing us to calculate the scalar weights (w_{WC} and w_{CC}) of a linear model that combines the filtered outputs of the WCs and CCs to determine turning rate (Fig. 3c). We used linear regression to calculate these weights for wild-type animals responding to fast sinusoidal temperature changes above, near, and below preferred temperatures (Fig. 3d). We found that the WC and CC outputs are flexibly weighted in each temperature range. Each weight depends on the absolute temperature (Extended Methods). At high temperatures, WC output is weighted 4x more strongly than CC output (Fig. 3d, g). At low temperatures, CC output is weighted 2x more strongly than WC output (Fig. 3d, e). At preferred temperatures, WC and CC outputs are equally weighted (Fig. 3d, f).

The thermotaxis algorithm explains how WC and CC outputs are effectively used to regulate behavior. During cold avoidance, turning during cooling is stimulated by the CCs and cross-inhibited by the WCs (Fig. 3e), resulting in a net increase in turning during cooling (Fig. 3h left). During warm avoidance, turning during warming is stimulated by the WCs and cross-inhibited by the CCs (Fig. 3g), resulting in a net increase in turning during warming (Fig. 3h right). Near preferred temperatures, turning during warming and cooling are mutually inhibited by the WCs and CCs (Fig. 3f), resulting in smaller turning rates during cooling and warming (Fig. 3h center). These rules amount to a cross-inhibitory algorithm that combines the simultaneous outputs of all thermosensory cells to generate thermotaxis.

The thermotaxis algorithm relies on the convolution of WC and CC neural responses with the filters to predict turning rate. These filters are biphasic in that they have both positive and negative parts (Fig. 3c). Biphasic filters are sensitive to the speed of the input signal;[29] therefore, we use fast and slow sinusoidal temperature waves in the behavioral experiments to compare to the algorithm predictions.

To test the algorithm, we used the weights measured using wild-type larvae responding to fast and slow sinusoidal temperature changes to predict the results of other experiments in which specific subsets of thermoreceptors were inactivated by mutation. Introducing non-functional mutations for receptors that are required for warming ($Ir68a^{PB}$) or cooling sensing ($Ir21a^{123}$) is equivalent to calculating the output of the cross-inhibition algorithm without WCs or CCs (Fig. 4a, b). Using a mutant for Ir93a ($Ir93a^{MI}$) –a receptor only expressed in WCs and CCs and required for their thermosensitivity– is equivalent to measuring the behavioral responses in the absence of the WCs' and CCs' thermosensory pathways. Therefore, the experimentally measured behavioral responses of $Ir93a^{MI}$ mutants are the baseline turning rate of the behavioral algorithm. We compared the predictions of our behavioral algorithm with the experimentally measured behavioral responses of mutant animals that lacked functional receptors in either the WCs, CCs, or both cell types. As predicted, inactivating WCs (via the $Ir68a^{PB}$ mutation) reduced turning during warming at high temperatures (Fig. 4g) and also reduced cross-inhibition of turning during cooling at preferred and low temperatures (Fig. 4c-f). As predicted, inactivating CCs (via the $Ir21a^{123}$ mutation) reduced turning during cooling at low temperatures (Fig. 3c, d) and reduced cross-inhibition of turning during warming at preferred and high temperatures (Fig. 3e, f, g). Inactivating both WCs and CCs (by the $Ir93a^{MI}$ mutation) caused thermal blindness at preferred temperatures (Fig. 4e, f). However, inactivating both WCs and CCs did not fully abolish behavioral responses at low or high temperatures. These residual responses are likely due to parallel thermosensory pathways that operate far from the preferred temperatures, constituting an additive correction to the algorithm implemented by the WCs and CCs (Fig. 4e-h and Extended Methods).

While the goal of the thermotaxis algorithm derived here is to capture the polarity and intensity of behavioral responses, it also successfully approximates the dynamics of the behavioral responses of wildtype and mutant animals, with correlation coefficients between 0.65 and 0.95 (Supplementary Fig. 10).

Discussion

Behavioral algorithms are often inferred from single behavioral responses to single stimulus types in specific environmental contexts.[4,9,11,12,17] Understanding animal behavior requires

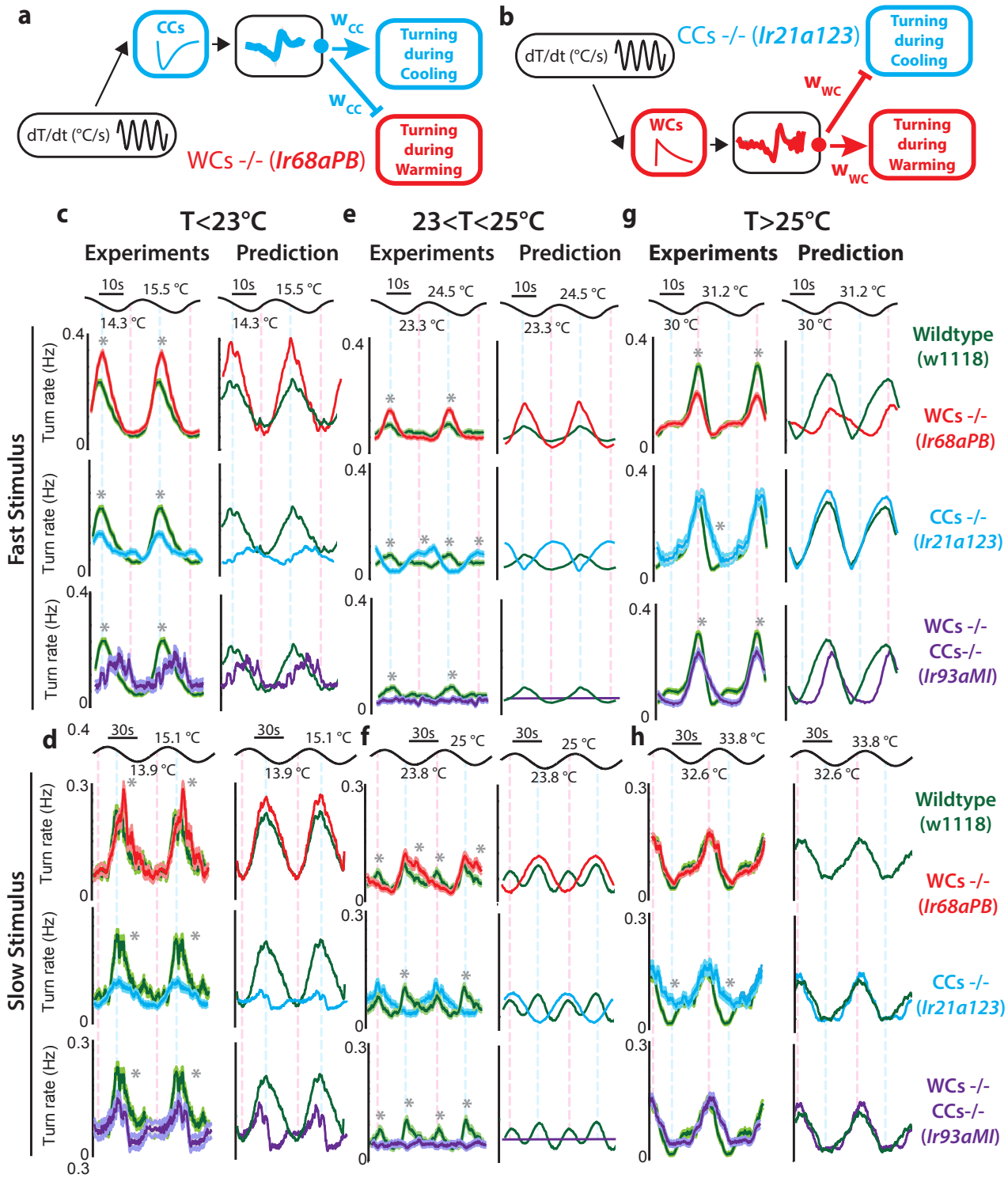

Figure 4. Flexible cross-inhibition between cooling and warming pathways controls thermotaxis. **a**, Schematic representation of the algorithm for thermotactic decision-making for larvae defective for WCs function (w^{1118}; $Ir68a^{PB}$). **b**, Schematic representation of the algorithm for thermotactic decision-making for larvae defective for WCs function (w^{1118}; $Ir21a^{123}$). **c-h left**, Experimental results of the turning rate response to fast (**c**, **e**, **g**) and slow (**d**, **f**, **h**) sine waves of temperature of wildtype larvae (w^{1118} in green), larvae defective for CCs' function (w^{1118}; $Ir21a^{123}$ in cyan, larvae defective for WCs' function (w^{1118}; $Ir68a^{PB}$ in red), and larvae defective for WCs and CCs function (w^{1118}; $Ir93a^{MI05555}$ in purple. Shaded regions are the s.e.m. * indicate different mean turning rate during cooling or warming using Chi-squared test with Bonferroni correction ($p<0.005$). **c-h right**, Quantitative predictions of the turning rate response to a fast (**c**, **e**, **g**) or slow (**d**, **f**, **h**) sine wave of temperature . Wildtype larvae's turning rate in green, larvae defective for WCs' function in red, larvae defective for CCs' function in cyan, and larvae defective for WCs and CCs function in purple. w^{1118} in green, n=80 in **c**, n=59 in **d**, n=50 in **e**, n=75 in **f**, n=62 in **g**, and n=72 in **q1**. w^{1118}; $Ir21a^{123}$ in cyan, n=45 in **c**, n=70 in **d**, n=54 in **e**, n=73 in **f**), n=49 in **g**, and n=81 in **h**. w^{1118}; $Ir68a^{PB}$ in red, n=61 in **c**, n=78 in **d**, n=59 in **e**, n=73 in **f**, n=55 in **g**, and n=77 in **h**. w^{1118}; $Ir93a^{MI05555}$ in purple, n=42 in **c**, , n=65 in **d**, n=45 in **e**, n=59 in **f**, n=55 in **g**, and n=70 in **h**.

considering the neural responses of multiple types of sensors and motor responses in different contexts. In sensory modalities that use opponent sensors to encode environmental stimuli, like photosensation, hygrosensation and thermosensation, often one sensor has been studied without its counterpart, making our understanding of that sensory modality incomplete.[4,7,17] In thermosensation, the justification for studying sensory cells function without their counterparts has been largely supported by the labeled line hypothesis in which each sensory cell type couples to a specific thermal stimulus and to a motor response

that leads the animal to safety or preferred temperatures.[1,31,32] In this view, the outputs of different sensory cells do not necessarily integrate to shape behavior. However, recent work in *Drosophila* has uncovered surprisingly complex thermosensory representations that are difficult to reconcile with simple hot and cold labeled lines.[33,34] In the *Drosophila* larva, both cooling cells (CCs) and newly discovered warming cells (WCs) respond in broad and overlapping temperature ranges that extend both above and below preferred temperatures. This means that warming and cooling cells are simultaneously active at high temperatures where warming should be avoided and at low temperatures where cooling should be avoided. In adult *Drosophila*, interneurons that explicitly integrate both cooling and warming signals have recently been characterized.[33,34] How might brains use different and simultaneously active sensors to compute behavior in different contexts? Here, we leveraged the robust thermal preference, small thermosensory system, and simple motor programs of the *Drosophila* larva to uncover new sensors and algorithms for context-dependent choice during thermotaxis.

We found that the larva integrates the output of WCs and CCs to compute behavioral responses. Genetic and cellular analysis revealed significant similarities between the opponent sensors. Each sensor requires a distinct but partly overlapping set of Ionotropic Receptors to detect temperature changes. The WCs require Ir68a, Ir93a, and Ir25a to detect warming. The CCs require Ir21a, Ir93a, and Ir25a to detect cooling. These distinct thermosensory properties of the WCs and CCs are encoded in their heteromeric expression of sets of Ir receptors. These Ionotropic Receptors are conserved across insects[35] and have homologs in the disease vector mosquitoes *Anopheles gambiae* and *Aedes aegypti*, which use temperature cues to identify human hosts.[36,37]

We individually characterized and quantified the temperature sensitivity and behavioral contributions of the WCs and CCs. Using calcium imaging, we mapped how temperature changes determine the activity of the WCs and CCs. Using quantitative behavioral analysis, we mapped how temperature changes determine motor response patterns. Using optogenetics, we mapped how the separate activity patterns of each sensor determine motor responses. These multilevel measurements allowed us to identify a thermotaxis algorithm that integrates the simultaneous outputs of the WCs and CCs at all temperatures.

We found that the larva uses a flexible cross-inhibitory algorithm to determine motor responses to temperature changes. Above 24°C warming is unfavorable because it carries the animal further from preferred temperatures. In this temperature range, avoidance responses during warming are stimulated by WCs and cross-inhibited by CCs. Below 24°C, cooling is unfavorable. In this temperature range, avoidance responses during cooling are stimulated by CCs and cross-inhibited by WCs. Near 24°C, both warming and cooling have neutral valence, and balanced cross-inhibition from WCs and CCs suppresses avoidance responses.

In perceptual choice models, cross-inhibition between competing groups of neurons often enhances accuracy in decision-making. In these model, such as the Usher-McClelland model of primate decision-making, different neuron groups are used to represent different choices.[38] These neurons mutually cross-inhibit their output pathways. The most strongly activated group that represents a specific choice thus biases the decisions towards one outcome by suppressing all others.[38,39] In the larva, the choice is whether to avoid cooling or warming: at high temperatures, warming should be avoided; at low temperatures cooling should be avoided. At all temperatures, however, the CCs are always more active during cooling and the WCs are always more active during warming. Thus, any cross-inhibition in the outputs of the WCs and CCs has to be flexible for these neurons to contribute differently to behavior in different contexts.

Here, we have uncovered the flexible cross-inhibition algorithm that drives *Drosophila* larva thermotaxis. At different temperatures, the algorithm assigns different weights to the outputs of opponent thermosensory cells. Assigning more weight to the output of either set of opponent sensors simultaneously increases its direct regulation of the avoidance response and cross-inhibits that of the other set. At preferred temperatures, cross-inhibition is balanced to suppress avoidance responses to temperature changes. At higher or lower temperatures, imbalanced cross-inhibition allows warm or cold avoidance to emerge. Understanding how the larval brain implements flexible cross-inhibition in neural circuits will require mapping downstream pathways using connectomics and physiology. Because cross-inhibition emerges from the polarity of the sensors themselves, their bidirectional phasic responses, and the linear model that transforms WC and CC activity into turning responses, it would suffice for the brain to linearly sum the outputs of the WCs and CCs to implement this algorithm. Our findings set the stage for studying how brain circuits implement flexible cross-inhibition in a decision-making algorithm.

Methods

Fly husbandry

Flies were raised at constant temperature (22 °C) and 50% humidity on standard cornmeal agar-based medium. For experiments with larvae, adult *Drosophila melanogaster* were transferred to collection cages (Genesee Scientific). One end of the cage held a grape juice agar plate and fresh yeast paste. Flies laid eggs on the agar plate for 2 days when the plate was removed to collect larvae. For all experiments, early second instar larvae were selected based on spiracle development using a dissection microscope.

Genotypes

The genotypes of fly stocks used in this study:

Effectors: UAS-GCaMP6m in the second chromosome: w[1118]; P[y[+t7.7] w[+mC]=20XUAS-IVS-GCaMP6m]attP40 (from BDSC 42748). UAS-GCaMP6m in the third chromosome: w[1118]; PBacy[+mDint2] w[+mC]=20XUAS-IVS-GCaMP6mVK00005 (from BDSC 42750). UAS-GFP: w[*]; P[y[+t7.7] w[+mC]=10XUAS-IVS-mCD8::GFP]attP40 (from BDSC 32186). UAS-Ir68a and UAS-Ir93a from.[3] UAS-Ir25a from.[40] UAS-CsChrimson: w[1118]; Py[+t7.7] w[+mC]=20XUAS-IVS-CsChrimson.mVenusattP2 (from BDSC 55136).

Gal4-Drivers: pebbled-Gal4 from.[14] w[1118];P[Ir68a-Gal4]attp2 backcrossed from,[3] and w[1118]; Py[+t7.7] w[+mC]=GMR11F02-GAL4attP2 from BDSC 49828.

Mutants: Ir68a^{PB} from,[3] Ir93a^{MI05555} from,[17] Ir21a^{123} from,[16] Ir25a^{2} from,[27] Ir25a-BAC from

Confocal microscopy

All fluorescence imaging was performed using a spinning-disk confocal setup using a 60x 1.2-N.A water immersion objective (Nikon Instruments LV100; Andor). During functional imaging in response to temperature changes, thermal expansion of the objective lens was compensated using a piezoelectric element.[7] For each experiment, larvae were washed with water and partially immobilized under a cover slip.[7] The microscope stage was temperature controlled using a Peltier thermoelectric actuator (Custom Thermoelectric) controlled with an H-bridged power driver and a two-degrees-of-freedom PID control algorithm. This algorithm was implemented using a PID control module (Accuthermo Technologies) operated by custom code written in LabView (See Extended Methods). The Peltier element was cooled by flowing antifreeze through an attached water block. The antifreeze was kept at 8-10°C using a VWR chiller.

Thermotaxis behavioral apparatus

The thermotaxis behavioral apparatus was operated inside a dark enclosure to prevent any light from causing phototactic artifacts. The behavioral arena was mounted on vibration-damping legs to eliminate mechanical artifacts. Dark-field illumination was provided with custom-built infrared LED bars (λ 850nm) operated with 10% pulse width modulation to avoid heating artifacts. The behavioral arena was temperature controlled with four Peltier thermoelectric actuators (Custom Thermoelectric) controlled with an H-bridged power driver and a two-degrees-of-freedom PID control algorithm. This algorithm was implemented with PID control modules (Accuthermo Technologies) and custom code written in LabView (See Extended Methods). Feedback signals for PID control were from thermocouples located in the behavioral arena as well as on the agar.

During behavioral experiments 15-18 larvae crawled freely for 20 min on 10x10 cm agar squares with 4mm thickness. These surfaces contained 2% agar and 0.1% activated charcoal (Sigma-aldrich). Charcoal is used to increase contrast for imaging with a CCD camera (Mightex) with a long-pass infrared filter (740nm) at 4 fps.

Optogenetic behavioral apparatus

For optogenetic experiments, animals were reared in cages with grape juice plates with a mixture of 0.18 grams of yeast and 400 uL of 0.5mM all-trans-retinal (ATR). The cages were kept in complete darkness until the experiment. The setup for optogenetic behavioral experiments is described elsewhere ([29]). In brief, optogenetic light stimulation was provided by a custom built LED matrix (SMD 5050 flexible LED strip lights, 12V DC, λ625nm). Optogenetic stimulation was controlled with an H bridge driver and custom code written for a LabJack U3 controller. Light intensity was controlled via pulse-width-modulation at 500kHz. Optogenetic stimulation was synchronized with image acquisition. Dark-field illumination was provided using custom-built infrared LED light bars (λ = 850nm). The wavelength of infrared illumination was chosen to avoid interference with the red LED illumination for optogenetic stimulation. Infrared LEDs for dark field illumination were mounted using opto-mechanical elements to adjust the angle with respect to the behavioral arena, avoiding larval 'shadows' that lowered the efficiency of data acquisition. The red LEDs were connected in parallel to produce uniform illumination. We verified uniform light intensity at 1.5 W/m2 +/- 0.02. The behavioral arena was 22x22 cm and used the same agar composition as for thermotaxis behavior experiments. In each experiment, 25-30 larvae were used and their movements were recorded with a CCD camera with a long-pass infrared filter (740nm) at 4 fps. Temperature was controlled in the same way as for thermotaxis behavior experiments.

Focused ion beam scanning electron microscopy (FIB-SEM)

For FIB-SEM serial sectioning, second third instar wild type Canton S larvae were used. After rinsing in PBS, the anterior half of the larva was incubated in fixative (2% formaldehyde with 2.5% glutardialdehyde in 0.1 M Na-cacodylate buffer, pH 7.4, Sigma-Aldrich, Germany,) for 30–90 min. Then, the head region was cut off and incubated in fresh fixative for 90 min. Samples were washed in Na-cacodylate, followed by post-fixation in 1% osmium tetroxide (SERVA Electrophoresis GmbH, Germany) for 2 hr at 48°C in the dark. En bloc staining was carried out with 1% uranyl acetate and 1% phosphotungstic acid in 70% EtOH in the dark over night before continuing the alcohol dehydration the next day. Samples were transferred to propylene oxide before embedded in Spurr (Plano,GmbH, Germany) using ascending Spurr concentrations diluted in propylene oxide for optimal tissue infiltration. Polymerization was carried out at 65°C for 72 hr. Blocks were trimmed using an Ultracut UCT microtome (Leica, Germany), mounted on conventional SEM stubs, and sputtered with 80–100 nm platinum. FIB-SEM serial sectioning was carried out using a FESEM Auriga Crossbeam workstation (Zeiss, Germany). FIB fine milling was carried out with 500 pA.

Behavioral quantification

Behavior was pre-processed using MAGAT Analyzer (https://github.com/samuellab/MAGATAnalyzer). Every larva image was used to calculate its mid-line. Each mid-line was then segmented in 11 points. Eight behavioral parameters where calculated from the body contour and segmented mid-line: speed, crab-speed, spine length, direction of motion, forward/backward crawling bias, head turn, head angular speed, and area of the larvae body (see extended methods for details). The time traces of these behavioral parameters over one period of a temperature sine wave stimulus were used to build an interpoint dissimilarity matrix, followed by multidimensional scaling, dimension selection, and an iterative denoising trees algorithm to classify larvae motor sequences in response to temperature fluctuations. This procedure was implemented following.[41] See the details of the calculations in the Extended Methods.

Thermotaxis model

One component of a thermotaxis algorithm is the filter that transforms the neural activity of CCs or WCs into behavioral responses. We estimated these filters by combining results from our calcium imaging experiments and optogenetic behavior experiments (see Extended Methods and[29]). In brief, the normalized measured activity responses of WCs and CCs (measured by calcium imaging) were convolved with the linear filters that convert WC and CC activities into behavioral responses (measured using optogenetics and quantitative behavioral analysis).

The result of these convolutions were weighted to reflect the contribution of each sensor type to behavioral response as follows:

$$Rcc_{turn}(t) = \int_0^\infty Hcc_{turn}(\tau) s_{CC}(t-\tau) d\tau \quad (1)$$

$$Rwc_{turn}(t) = \int_0^\infty Hwc_{turn}(\tau) s_{WC}(t-\tau) d\tau \quad (2)$$

Where Hwc_{turn} and Hcc_{turn} are the convolution kernels for the WCs and CCs, respectively. Each kernel is computed from the signal history of the WCs ($s_{WC}(t-\tau)$) and CCs ($s_{CC}(t-\tau)$).

The turning rates calculated from equations (1) and (2) are linearly combined with scalar weights, w_{CC} and w_{WC}, to obtain the predicted turning rate $R_{turn}(t)$ as follows:

$$R_{turn}(t) = w_{CC} * Rcc_{turn}(t) + w_{WC} * Rwc_{turn}(t) \quad (3)$$

Because w_{CC} and w_{WC} capture the relative contributions of the CCs and WCs we parametrize them to vary between 0 and 1 with a fixed scaling factor k, such that:

$$w_{CC} = k * (w) \quad (4)$$

$$w_{WC} = k * (1-w) \quad (5)$$

When w is 0, $w_{CC} = 0$ and behavior is entirely driven by the WCs. When w is 0.5, $w_{CC} = w_{WC} = k/2$ and behavior has equal contributions from WCs and CCs. When w is 1, $w_{WC} = 0$ and behavior is entirely driven by the CCs. The fixed scalar parameter k sets the scale of the predicted turning responses. The weights are determined as follows. First, w is fitted by linear regression assuming $k = 1$ and normalizing the amplitude of the predicted and experimentally measured responses – this step fits the shape of the response. Second, k is linearly regressed to match the amplitude of the responses. The predicted turning rate is passed through a saturation function to guarantee positive values.

ACKNOWLEDGEMENTS

We acknowledge members of the Samuel for helpful discussions and comments on the manuscript. We thank Rachel Wilson, Sandeep Robert Datta, and Alex Schier for helpful discussions and advice during the development of the project. We acknowledge the Bloomington *Drosophila* Stock Center (NIH P40OD018537). L.H-N., G.B., P.G. and A.D.T.S. were supported by the NIH R01 GM130842-01 grant. A.S.T., V.R. and A.R., were supported by the Deutsche Forschungsgemeinschaft (TH1584/3-1, TH1584/6-1 and TH1584/7-1).

AUTHOR CONTRIBUTIONS

L.H-N. developed the experimental techniques for temperature control and optogenetics, wrote the software for behavioral classification, analyzed data, performed behavioral experiments, functional and anatomical imaging, and optogenetic experiments, and derived the thermotaxis behavioral algorithm. A.C. performed behavioral experiments, functional imaging, and optogenetic experiments. G.B. conducted immunostaining and anatomy experiments. V.R., A.R. and A.S.T. contributed the EM dataset and did the EM reconstruction. M.K. provided reagents and preliminary data. L. H-N., P.G. and A.D.T.S. designed the study, interpreted the results, and wrote the manuscript with feedback from all authors.

COMPETING INTERESTS

The authors declare no competing interests.

References

[1] Marco Gallio, Tyler A Ofstad, Lindsey J Macpherson, Jing W Wang, and Charles S Zuker. The coding of temperature in the drosophila brain. *Cell*, 144(4):614–624, 2011.

[2] Raf J Schepers and Matthias Ringkamp. Thermoreceptors and thermosensitive afferents. *Neuroscience & Biobehavioral Reviews*, 34(2):177–184, 2010.

[3] Zachary A Knecht, Ana F Silbering, Joyner Cruz, Ludi Yang, Vincent Croset, Richard Benton, and Paul A Garrity. Ionotropic receptor-dependent moist and dry cells control hygrosensation in drosophila. *Elife*, 6:e26654, 2017.

[4] Anders Enjin, Emanuela E Zaharieva, Dominic D Frank, Suzan Mansourian, Greg SB Suh, Marco Gallio, and Marcus C Stensmyr. Humidity sensing in drosophila. *Current Biology*, 26(10):1352–1358, 2016.

[5] Wei Li and Steven H DeVries. Bipolar cell pathways for color and luminance vision in a dichromatic mammalian retina. *Nature neuroscience*, 9(5):669–675, 2006.

[6] Edward V Famiglietti, Akimichi Kaneko, and Masao Tachibana. Neuronal architecture of on and off pathways to ganglion cells in carp retina. *Science*, 198(4323):1267–1269, 1977.

[7] Mason Klein, Bruno Afonso, Ashley J Vonner, Luis Hernandez-Nunez, Matthew Berck, Christopher J Tabone, Elizabeth A Kane, Vincent A Pieribone, Michael N Nitabach, Albert Cardona, et al. Sensory determinants of behavioral dynamics in drosophila thermotaxis. *Proceedings of the National Academy of Sciences*, 112(2):E220–E229, 2015.

[8] Hans Jürgen Solinski and Mark A Hoon. Cells and circuits for thermosensation in mammals. *Neuroscience letters*, 690:167–170, 2019.

[9] Belinda Barbagallo and Paul A Garrity. Temperature sensation in drosophila. *Current Opinion in Neurobiology*, 34:8–13, 2015.

[10] Miriam B Goodman and Piali Sengupta. The extraordinary afd thermosensor of c. elegans. *Pflügers Archiv-European Journal of Physiology*, 470(5):839–849, 2018.

[11] Martin Haesemeyer, Drew N Robson, Jennifer M Li, Alexander F Schier, and Florian Engert. A brain-wide circuit model of heat-evoked swimming behavior in larval zebrafish. *Neuron*, 98(4):817–831, 2018.

[12] Martin Haesemeyer, Drew N Robson, Jennifer M Li, Alexander F Schier, and Florian Engert. The structure and timescales of heat perception in larval zebrafish. *Cell systems*, 1(5):338–348, 2015.

[13] Tsai-Wen Chen, Trevor J Wardill, Yi Sun, Stefan R Pulver, Sabine L Renninger, Amy Baohan, Eric R Schreiter, Rex A Kerr, Michael B Orger, Vivek Jayaraman, et al. Ultrasensitive fluorescent proteins for imaging neuronal activity. *Nature*, 499(7458):295–300, 2013.

[14] Lora B Sweeney, Africa Couto, Ya-Hui Chou, Daniela Berdnik, Barry J Dickson, Liqun Luo, and Takaki Komiyama. Temporal target restriction of olfactory receptor neurons by semaphorin-1a/plexina-mediated axon-axon interactions. *Neuron*, 53(2):185–200, 2007.

[15] Eftychios A Pnevmatikakis, Daniel Soudry, Yuanjun Gao, Timothy A Machado, Josh Merel, David Pfau, Thomas Reardon, Yu Mu, Clay Lacefield, Weijian Yang, et al. Simultaneous denoising, deconvolution, and demixing of calcium imaging data. *Neuron*, 89(2):285–299, 2016.

[16] Lina Ni, Mason Klein, Kathryn V Svec, Gonzalo Budelli, Elaine C Chang, Anggie J Ferrer, Richard Benton, Aravinthan DT Samuel, and Paul A Garrity. The ionotropic receptors ir21a and ir25a mediate cool sensing in drosophila. *Elife*, 5:e13254, 2016.

[17] Zachary A Knecht, Ana F Silbering, Lina Ni, Mason Klein, Gonzalo Budelli, Rati Bell, Liliane Abuin, Anggie J Ferrer, Aravinthan DT Samuel, Richard Benton, et al. Distinct combinations of variant ionotropic glutamate receptors mediate thermosensation and hygrosensation in drosophila. *Elife*, 5:e17879, 2016.

[18] Gonzalo Budelli, Lina Ni, Cristina Berciu, Lena van Giesen, Zachary A Knecht, Elaine C Chang, Benjamin Kaminski, Ana F Silbering, Aravi Samuel, Mason Klein, et al. Ionotropic receptors specify the morphogenesis of phasic sensors controlling rapid thermal preference in drosophila. *Neuron*, 101(4):738–747, 2019.

[19] Bryce L MUNGER and Chizuka IDE. The structure and function of cutaneous sensory receptors. *Archives of histology and cytology*, 51(1):1–34, 1988.

[20] Hao Wu, John Williams, and Jeremy Nathans. Morphologic diversity of cutaneous sensory afferents revealed by genetically directed sparse labeling. *Elife*, 1:e00181, 2012.

[21] RF Foelix, RF Stocker, and RA Steinbrecht. Fine structure of a sensory organ in the arista of drosophila melanogaster and some other dipterans. *Cell and tissue research*, 258(2):277–287, 1989.

[22] Bertram Gerber and Reinhard F Stocker. The drosophila larva as a model for studying chemosensation and chemosensory learning: a review. *Chemical senses*, 32(1):65–89, 2007.

[23] Elizabeth C Marin, Ruairí JV Roberts, Laurin Büld, Maria Theiss, Markus W Pleijzier, Tatevik Sarkissian, Willem J Laursen, Robert Gillies Turnbull, Philipp Schlegel, Alexander Shakeel Bates, et al. Connectomics analysis reveals first, second, and third order thermosensory and hygrosensory neurons in the adult drosophila brain. *BioRxiv*, 2020.

[24] Youngseok Lee, Seeta Poudel, Yunjung Kim, Dhananjay Thakur, and Craig Montell. Calcium taste avoidance in drosophila. *Neuron*, 97(1):67–74, 2018.

[25] Floris van Breugel, Ainul Huda, and Michael H Dickinson. Distinct activity-gated pathways mediate attraction and aversion to co 2 in drosophila. *Nature*, 564(7736):420–424, 2018.

[26] Juan Antonio Sánchez-Alcañiz, Ana Florencia Silbering, Vincent Croset, Giovanna Zappia, Anantha Krishna Sivasubramaniam, Liliane Abuin, Saumya Yashmohini Sahai, Daniel Münch, Kathrin Steck, Thomas O Auer, et al. An expression atlas of variant ionotropic glutamate receptors identifies a molecular basis of carbonation sensing. *Nature communications*, 9(1):1–14, 2018.

[27] Richard Benton, Kirsten S Vannice, Carolina Gomez-Diaz, and Leslie B Vosshall. Variant ionotropic glutamate receptors as chemosensory receptors in drosophila. *Cell*, 136(1):149–162, 2009.

[28] Linjiao Luo, Marc Gershow, Mark Rosenzweig, KyeongJin Kang, Christopher Fang-Yen, Paul A Garrity, and Aravinthan DT Samuel. Navigational decision making in drosophila thermotaxis. *Journal of Neuroscience*, 30(12):4261–4272, 2010.

[29] Luis Hernandez-Nunez, Jonas Belina, Mason Klein, Guangwei Si, Lindsey Claus, John R Carlson, and Aravinthan DT Samuel. Reverse-correlation analysis of navigation dynamics in drosophila larva using optogenetics. *Elife*, 4:e06225, 2015.

[30] Nathan C Klapoetke, Yasunobu Murata, Sung Soo Kim, Stefan R Pulver, Amanda Birdsey-Benson, Yong Ku Cho, Tania K Morimoto, Amy S Chuong, Eric J Carpenter, Zhijian Tian, et al. Independent optical excitation of distinct neural populations. *Nature methods*, 11(3):338, 2014.

[31] Aziz Moqrich, Sun Wook Hwang, Taryn J Earley, Matt J Petrus, Amber N Murray, Kathryn SR Spencer, Mary Andahazy, Gina M Story, and Ardem Patapoutian. Impaired thermosensation in mice lacking trpv3, a heat and camphor sensor in the skin. *Science*, 307(5714):1468–1472, 2005.

[32] Ajay Dhaka, Amber N Murray, Jayanti Mathur, Taryn J Earley, Matt J Petrus, and Ardem Patapoutian. Trpm8 is required for cold sensation in mice. *Neuron*, 54(3):371–378, 2007.

[33] Wendy W Liu, Ofer Mazor, and Rachel I Wilson. Thermosensory processing in the drosophila brain. *Nature*, 519(7543):353–357, 2015.

[34] Dominic D Frank, Genevieve C Jouandet, Patrick J Kearney, Lindsey J Macpherson, and Marco Gallio. Temperature representation in the drosophila brain. *Nature*, 519(7543):358–361, 2015.

[35] Vincent Croset, Raphael Rytz, Scott F Cummins, Aidan Budd, David Brawand, Henrik Kaessmann, Toby J Gibson, and Richard Benton. Ancient protostome origin of chemosensory ionotropic glutamate receptors and the evolution of insect taste and olfaction. *PLoS genetics*, 6(8), 2010.

[36] Roman A Corfas and Leslie B Vosshall. The cation channel trpa1 tunes mosquito thermotaxis to host temperatures. *Elife*, 4:e11750, 2015.

[37] Chloe Greppi, Willem J Laursen, Gonzalo Budelli, Elaine C Chang, Abigail M Daniels, Lena van Giesen, Andrea L Smidler, Flaminia Catteruccia, and Paul A Garrity. Mosquito heat seeking is driven by an ancestral cooling receptor. *Science*, 367(6478):681–684, 2020.

[38] Marius Usher and James L McClelland. The time course of perceptual choice: the leaky, competing accumulator model. *Psychological review*, 108(3):550, 2001.

[39] Thomas D Seeley, P Kirk Visscher, Thomas Schlegel, Patrick M Hogan, Nigel R Franks, and James AR Marshall.

Stop signals provide cross inhibition in collective decision-making by honeybee swarms. *Science*, 335(6064):108–111, 2012.

[40] Liliane Abuin, Benoîte Bargeton, Maximilian H Ulbrich, Ehud Y Isacoff, Stephan Kellenberger, and Richard Benton. Functional architecture of olfactory ionotropic glutamate receptors. *Neuron*, 69(1):44–60, 2011.

[41] Joshua T Vogelstein, Youngser Park, Tomoko Ohyama, Rex A Kerr, James W Truman, Carey E Priebe, and Marta Zlatic. Discovery of brainwide neural-behavioral maps via multiscale unsupervised structure learning. *Science*, 344(6182):386–392, 2014.

[42] Lena Van Giesen, Luis Hernandez-Nunez, Sophie Delasoie-Baranek, Martino Colombo, Philippe Renaud, Rémy Bruggmann, Richard Benton, Aravinthan DT Samuel, and Simon G Sprecher. Multimodal stimulus coding by a gustatory sensory neuron in drosophila larvae. *Nature communications*, 7(1):1–10, 2016.

[43] Helmut Altner and Richard Loftus. Ultrastructure and function of insect thermo-and hygroreceptors. *Annual review of entomology*, 30(1):273–295, 1985.

[44] Feng Ding, Yang Shi, and Tongwen Chen. Gradient-based identification methods for hammerstein nonlinear armax models. *Nonlinear Dynamics*, 45(1-2):31–43, 2006.

[45] Mituhiko Araki and Hidefumi Taguchi. Two-degree-of-freedom pid controllers. *International Journal of Control, Automation, and Systems*, 1(4):401–411, 2003.

[46] Joseph S Bell and Rachel I Wilson. Behavior reveals selective summation and max pooling among olfactory processing channels. *Neuron*, 91(2):425–438, 2016.

[47] Marc Gershow, Matthew Berck, Dennis Mathew, Linjiao Luo, Elizabeth A Kane, John R Carlson, and Aravinthan DT Samuel. Controlling airborne cues to study small animal navigation. *Nature methods*, 9(3):290, 2012.

[48] Shimaa AM Ebrahim, Hany KM Dweck, Johannes Stökl, John E Hofferberth, Federica Trona, Kerstin Weniger, Jürgen Rybak, Yoichi Seki, Marcus C Stensmyr, Silke Sachse, et al. Drosophila avoids parasitoids by sensing their semiochemicals via a dedicated olfactory circuit. *PLoS biology*, 13(12), 2015.